



# Geophysical Research Letters

## RESEARCH LETTER

10.1029/2019GL083420

### Special Section:

Atmospheric Rivers:  
Intersection of Weather and Climate

### Key Points:

- Landfalling frequency and genesis location of southern China typhoon are affected by different mechanisms during peak summer
- Interdecadal changes in landfalling typhoon (LFTY) genesis location are primarily attributed to the late-1990s Mega-La Niña-like regime shift
- Variations of LFTY frequency are mainly driven by the easterly steering flows near 20°N associated with the western North Pacific subtropical high activity

### Supporting Information:

- Supporting Information S1

### Correspondence to:

C. Hu,  
huchd3@mail.sysu.edu.cn

### Citation:

Zhang, C., Hu, C., Huang, G., Yao, C., Zheng, Z., Wang, T., et al. (2019). Perspective on landfalling frequency and genesis location variations of southern China typhoon during peak summer. *Geophysical Research Letters*, 46, 6830–6838. <https://doi.org/10.1029/2019GL083420>

Received 26 APR 2019

Accepted 20 MAY 2019

Accepted article online 28 MAY 2019

Published online 17 JUN 2019

<sup>†</sup>Chengyang Zhang and Chundi Hu contributed equally to the study and are co-first authors.

©2019. The Authors.

This is an open access article under the terms of the Creative Commons Attribution-NonCommercial-NoDerivs License, which permits use and distribution in any medium, provided the original work is properly cited, the use is non-commercial and no modifications or adaptations are made.

## Perspective on Landfalling Frequency and Genesis Location Variations of Southern China Typhoon During Peak Summer

Chengyang Zhang<sup>1</sup> , Chundi Hu<sup>2,3,4</sup> , Gang Huang<sup>4</sup> , Cai Yao<sup>1</sup>, Zhihai Zheng<sup>5</sup>, Teng Wang<sup>2</sup>, Zeming Wu<sup>2</sup>, Song Yang<sup>2,3,6</sup> , and Dake Chen<sup>3,7</sup>

<sup>1</sup>Climate Center & Guangxi Institute of Meteorological Sciences, Guangxi Meteorological Bureau, Nanning, China,

<sup>2</sup>School of Atmospheric Sciences & Guangdong Province Key Laboratory for Climate Change and Natural Disaster Studies, Sun Yat-sen University, Zhuhai, China, <sup>3</sup>Southern Marine Science and Engineering Guangdong Laboratory (Zhuhai), Zhuhai, China, <sup>4</sup>State Key Laboratory of Numerical Modeling for Atmospheric Sciences and Geophysical Fluid Dynamics, Institute of Atmospheric Physics, Chinese Academy of Sciences, Beijing, China, <sup>5</sup>Laboratory for Climate Studies, National Climate Center, China Meteorological Administration, Beijing, China, <sup>6</sup>Institute of Earth Climate and Environment System, Sun Yat-sen University, Guangzhou, China, <sup>7</sup>State Key Laboratory of Satellite Ocean Environment Dynamics, Second Institute of Oceanography, Ministry of Natural Resources, Hangzhou, China

**Abstract** Increasing intense landfalling typhoons (LFTYs) are of great coastal threats to southern China. However, changes in genesis location and landfalling frequency of western North Pacific (WNP) LFTY dedicated to southern China remain unclear. Here we identified such LFTYs during peak summer and found that most LFTYs formed south of 20°N and the LFTY genesis locations over southern WNP have also experienced a sharp interdecadal shift since 1998, which are mainly attributed to the large-scale environment changes induced by the Mega-La Niña-like climate shift. However, LFTY frequency (= “landfalling frequency of southern China typhoon”) shows a slight increasing trend but without significant interdecadal variation. Variations of LFTY frequency are mainly affected by the easterly steering flows near 20°N over the South China Sea and the Philippine Sea, which are closely linked to the WNP subtropical high activity. Our results provide a new perspective on the LFTY activities dedicated to southern China.

**Plain Language Summary** We explore the changes in frequency and genesis location of landfalling typhoon (LFTY) dedicated to southern China during peak summer over 1979–2015, which is important for people's life and property from the coastal risk perspective. Results show that the LFTY genesis location is primarily modulated by the Pacific interdecadal variation via modifying the large-scale atmospheric and oceanic responses over the western North Pacific. While the LFTY frequency (= “landfalling frequency of southern China typhoon”) is significantly affected by the easterly steering flows near 20°N over the South China Sea and the Philippine Sea, which are closely linked to the western North Pacific subtropical high activity.

## 1. Introduction

Intense tropical cyclone (TC) often takes strong storm-surge, heavy rainstorm and even coastal flooding (e.g., Seo & Bakkensen, 2017; Woodruff et al., 2013), with severe impacts on employment (Wu, 2019) and enormous socioeconomic risks/losses (Peduzzi et al., 2012) due to the accelerating sea-level rise (Woodruff et al., 2013). Especially for those super typhoons such as Billis (2000), Imbudo (2003), Haitang, Talim & Longwang (2005), Saomai (2006), Sepat (2007), Rammasan (2014), Nepartak, Meranti & Haima (2016), Maria & Mangkhut (2018), which have caused tremendous threats and damages to people's life and property along the South China coast. Such severe damage depends largely on the location where it makes landfall (Chan et al., 2019; Guo & Tan, 2018).

For the western North Pacific (WNP), increasing proportion and destructiveness of landfalling typhoon (LFTY) striking southern China has caused great climate concerns on the TC-climate research (e.g., Knutson et al., 2010; Li et al., 2017; Mei & Xie, 2016; Zhan et al., 2017). It is found that locally robust sea surface temperature (SST) warming in the WNP strongly contributes to the increased rapid-intensification of LFTY and the rate of intense TCs (Mei et al., 2015; Mei & Xie, 2016; Zhan et al., 2017; J. Zhao, Zhan, & Wang, 2018). The WNP SST warming is mainly induced by the Pacific decadal oscillation (PDO)-,

Interdecadal Pacific oscillation (IPO)- and/or Mega-La Niña-related climate shift since the late-1990s (e.g., Hong et al., 2016; C. Hu, Zhang, et al., 2018; Zhan et al., 2017; J. Zhao, Zhan, Wang, & Xu, 2018; H. Zhao, Duan, et al., 2018).

Besides, the late-1990s Pacific regime shift also contributes to the northwestward shift of WNP TC genesis location during autumn (C. Hu, Zhang, et al., 2018). Zhan et al. (2017) suggest that intense TCs formed over the western WNP have stronger coastal risk than those formed over the eastern WNP. However, despite an increase in typhoon intensity with local SST warming, the reduced developing duration (due to the northwestward shift of TC genesis location) and decreased TC frequency (e.g., He et al., 2015; F. Hu, Li, et al., 2018; Maue, 2011; Takahashi et al., 2017) tend to offset the increasing TC intensity from a typhoon destructive potential perspective (Lin & Chan, 2015), often with conflicting effects (Knutson et al., 2010). Meanwhile, there are significant westward expansions of WNP subtropical high (WNPSH) since the 1950s (Wu & Wang, 2015) and tropical upper tropospheric trough (TUTT) since the late-1970s (Wang & Wu, 2016, 2018; Wu et al., 2015), which are closely linked to the changes in steering flow and genesis location of TC, respectively.

Accordingly, whether above climate changes give rise to the variations of landfalling frequency and genesis location of typhoon striking southern China remain unclear and deserve investigate separately, which is of great concern in present study. The following results will reveal that the mean genesis location of southern China LFTYs also shows a pronounced northwestward shift since late-1990s, whereas changes in LFTY frequency (= “landfalling frequency of southern China typhoon”) are moderate in comparison; and the relevant potential mechanisms are discussed, respectively.

## 2. Data and Methodology

Previous studies pointed out that the TC best-track datasets from the Joint Typhoon Warning Center (JTWC, [https://metoc.ndbc.noaa.gov/web/guest/jtvc/best\\_tracks/](https://metoc.ndbc.noaa.gov/web/guest/jtvc/best_tracks/)) are relatively more reliable than those from other datasets (e.g., Chan, 2008; Mei & Xie, 2016; Wu & Zhao, 2012). Moreover, increasing TC-related climate studies primarily use the JTWC data to show their new findings (e.g., Hong et al., 2011; Zhao & Wu, 2014; Mei et al., 2015; Zhan et al., 2017; Guo & Tan, 2018; H. Zhao, Duan, et al., 2018; C. Hu, Zhang, et al., 2018; Hu et al., 2019; J. Zhao, Zhan, Wang, & Xu, 2018; J. Zhao, Zhan, & Wang, 2018). Accordingly, the JTWC TC datasets are also primarily employed in this study. Because only about one-fifth of TCs (with the intensity of a hurricane defined by maximum sustained wind speeds  $\geq 33$  m/s) make landfall, but coastal impacts are due to this important subset of typhoons to a large extent (e.g., Weinkle et al., 2012; Woodruff et al., 2013). Thus here we only focus on the southern China LFTYs (refer to any typhoon that crosses the coastline of China between  $20^{\circ}\text{N}$ - $30^{\circ}\text{N}$ ) with 1-min maximum sustained winds  $\geq 64$  knots (about 33 m/s, 1 knot  $\approx 0.511$  m/s) in peak summer (i.e., July–September, JAS) during 1979–2015.

Monthly atmospheric data are obtained from the Interim European Centre for Medium-range Weather Forecasts Reanalysis (Dee et al., 2011). The following two monthly SST datasets are averaged before using in this study since the mean SST data favors offsetting their inconsistent signal/noise to certain extent (Hu et al., 2016): the National Oceanic and Atmospheric Administration Extended Reconstructed SST version 4 ( $2^{\circ} \times 2^{\circ}$ , Huang et al., 2015) and the Hadley Centre SST (interpolated to the same  $2^{\circ} \times 2^{\circ}$  grid, Rayner et al., 2003). The PDO index is directly downloaded from <http://research.jisao.washington.edu/pdo/> and the ENSO index [represented by the Oceanic Niño Index (ONI)] is obtained from <http://www.cpc.ncep.noaa.gov/data/indices/oni.ascii.txt>. The IPO and Mega-ENSO indices separately defined by Henley et al. (2015) and Wang et al. (2013) are also used. The empirical orthogonal function (EOF) analysis [also called principle component (PC) analysis] is employed to capture the leading modes of the regional steering flow (simply represented by the mean zonal wind averaged from 925 hPa to 700 hPa).

## 3. Results

### 3.1. Changes in Southern China LFTY Activities

Figure 1(a) shows that less than 1/3 (only 31.9%) of typhoons make landfall over southern China even in the most active typhoon season (JAS) during 1979–2015. There are 107 LFTYs in total, as shown in Figure 1(b), and most of them form at south of  $20^{\circ}\text{N}$ , over the southwest of WNPSH (i.e.,  $5^{\circ}\text{N}$ - $20^{\circ}\text{N}$ ,  $115^{\circ}\text{E}$ - $160^{\circ}\text{E}$ ).

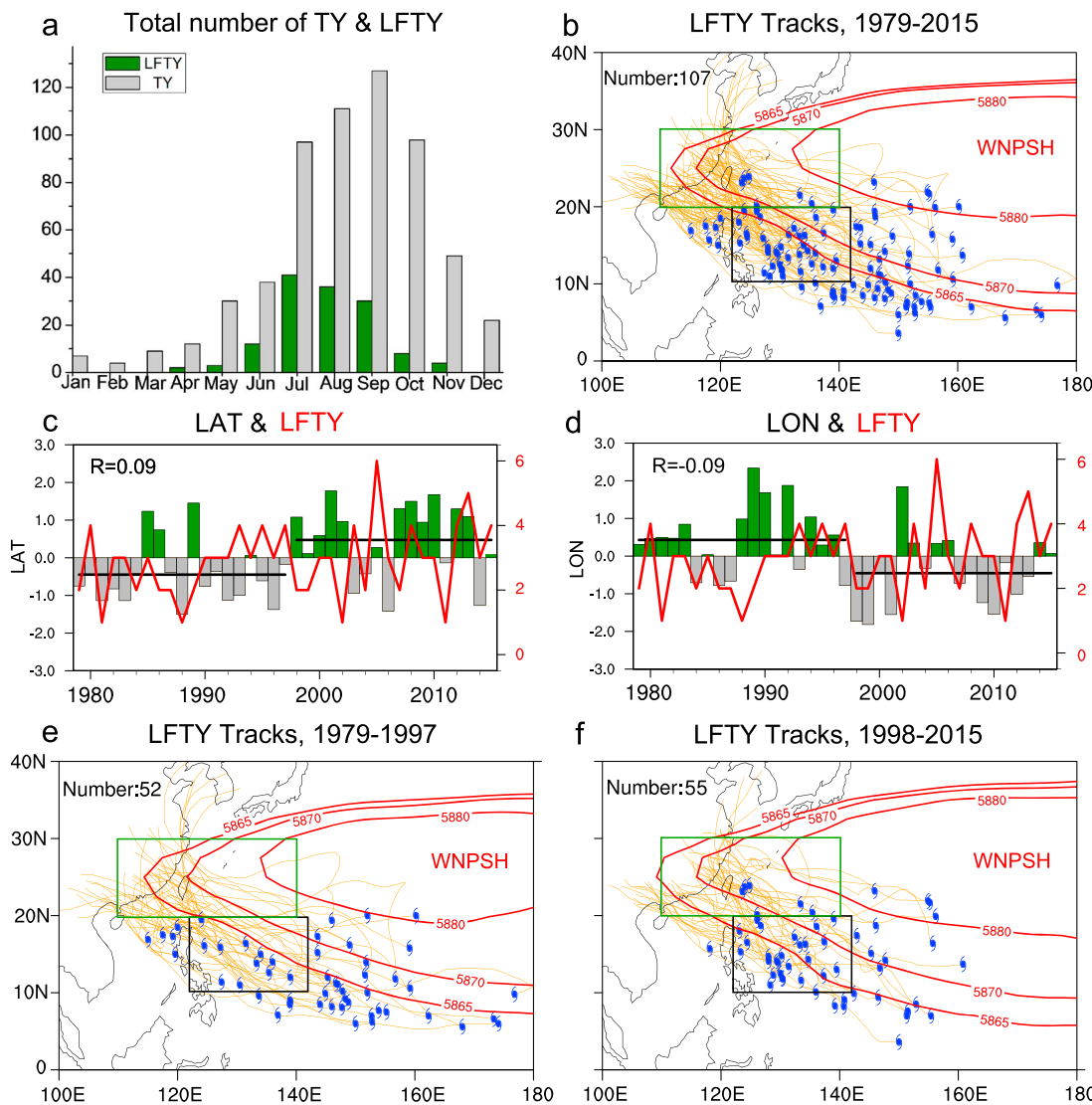


**Figure 1.** (a) monthly mean of southern China LFTY and all WNP typhoon (TY) frequencies. (b) moving tracks and genesis locations of LFTY and the WNPSH (red contours) during JAS for 1979–2015. Shown in (c) and (d) are the normalized time series (bar) of the mean latitude (LAT) and longitude (LON) of southern China LFTY genesis location. Also shown in (c) and (d) are the southern China LFTY frequency (orange line). Shown in (e) and (f) are same as in (b) except for 1979–1997 and 1998–2015, respectively. The green and black boxes in (b), (e) and (f) indicate the same reference systems for the relative position of the WNPSH and LFTY, respectively.

Besides, the LFTY tracks are well corresponded to the steering flows along the southwest flank of WNPSH, which tend to steer the typhoon northwestward shift to southern China (Figure 1(b)).

Previous studies have pointed out that increasing weak TCs formed over the northwestern WNP mainly induced by the locally SST warming and greater warming at higher latitudes associated with global warming (Zhan & Wang, 2017) and/or the PDO/IPO/Mega-La Nina-like regime shifts (e.g., He et al., 2015; Mei & Xie, 2016; C. Hu et al., 2018; Zhan et al., 2017; J. Zhao, Zhan, Wang, & Xu, 2018; J. Zhao, Zhan, & Wang, 2018), contributing to the poleward shift of the annual mean location of the WNP TCs. Of note is that the weak TCs are mainly distributed north of  $20^{\circ}\text{N}$  (He et al., 2015). Here, we further find that both the latitude and longitude of LFTY genesis locations (south of  $20^{\circ}\text{N}$ ) also generally reflect a remarkable interdecadal change in late-1990s (Figures 1(c)-1(d); Table S1).

For a more detailed comparison, Figures 1(e)-1(f) show the genesis locations and tracks of LFTYs with the corresponding climatology of WNPSH before and after late-1990s (hereafter period-I and period-II),

respectively. As expected, there are much more LFTYs formed in the Philippine Sea (see the black-box in Figure 1(f):  $10^{\circ}\text{N}$ - $20^{\circ}\text{N}$ ,  $122^{\circ}\text{E}$ - $142^{\circ}\text{E}$ ) during period-II, but significant less LFTYs formed in the South China Sea (westernmost WNP) and the southeastern WNP relative to the period-I (Figure 1(e)). Meanwhile, the enhanced WNPSH expands westward to southern China during period-II (Figure 1(f)) from the climatology perspective, which steering relatively more LFTYs toward southern China during period-II correspondingly. However, there seems to be no any relationship between LFTY frequency and variations of LFTY genesis location ( $R \approx 0$ , Figures 1(c)-1(d)), indicating that they are affected by different factors.

### 3.2. Potential Mechanisms

According to previous studies, the interdecadal shifts of WNP TC genesis location are importantly indicated by the changes in large scale oceanic and atmospheric environments, especially the horizontal distribution of SST anomalies, the east-west shift of TUTT and monsoon trough (MT), as well as the tropospheric vertical wind shear and mid-level relative humidity (e.g., Camargo et al., 2007; Huangfu et al., 2017; Zhao, Jiang, et al., 2015; Zhao, Yoshida, et al., 2015; Zhao & Wu, 2018). To further identify and confirm the large-scale environment changes associated with the interdecadal variations of LFTY genesis location, the relevant interdecadal change patterns are shown in Figure 2.

The most prominent feature is that significant SST warming (centered near the Japan) and cooling (centered near the Hawaii) in the North Pacific (Figures 2(a)-2(b)) are closely correlated to the interdecadal changes in the mean LFTY genesis location. Here we propose a North Pacific SST dipole index (NPD; see the Figure 2 caption for details) for these two SST anomaly centers, which is highly correlated to the PDO ( $r = -0.90$ , Figure 3) and IPO/Mega-ENSO ( $r = -0.84/0.75$ ; see Table S2, *note that the correlation of IPO and Mega-ENSO is  $-0.96$ , almost the same species*). And all of their time series exhibit a sharp interdecadal change in late-1990s (Figure 2(c)). Moreover, the patterns shown in Figures 2(a)-2(b) are also generally mirrored by the SST interdecadal differences, belonging to the K-shape SST anomaly mode related to PDO-like and/or IPO/Mega-La Niña backgrounds (Figure 2(d)), which might be responsible for the interdecadal variations of LFTY genesis location (Table S2).

Corresponding to such a PDO-related Mega-La Niña-like climate regime shift (Figure 2(d)), the weakened WNP anticyclone and intensified low-level easterly trade winds cause a northwestward retreat of MT (Figure 2(e)). Meanwhile, the upper-level positive vorticity anomalies induce a weakened south Asian high and a southwestward expanded TUTT (Figure 2(f)). This is consistent with C. Hu, Zhang, et al. (2018) that a southwestward shifting TUTT always corresponds to a northwestward retreating MT, as shown in Figures 2(e)-2(f). Note that the TUTT-MT index (see the Figure 2 caption for details) is well correlated to the PDO, IPO/Mega-ENSO, NPD, as well as the mean latitude and longitude of LFTYs, but not to the LFTY frequency (Figure 3 and Table S2). The corresponded changes in upper-level and low-level winds (Figures 2(e)-2(f)) together result in a large scale negative and positive vertical wind shears over the subtropical WNP and southeastern WNP (Figure 2(g)), respectively. In addition, the mid-level relative humidity (Figure 2(h)) gets wetter (west to  $170^{\circ}\text{E}$ ) and drier (east to  $170^{\circ}\text{E}$ ) due to the local SST warming and cooling (Figure 2(d)). Such large-scale dynamic and thermodynamic conditions favor more TCs (including LFTYs) forming over the northwestern WNP (Figures 1(e)-1(f)), ultimately contributing to the interdecadal changes of LFTY genesis location (Figures 1(c)-1(d)). Similar results can be corroborated by the comprehensive Genesis Potential Index changes (Figure S1; Emanuel & Nolan, 2004; Murakami & Wang, 2010).

Of note is that there is no significant interdecadal signal in the LFTY frequency (Figures 1(c)-1(d)); and the LFTY frequency has not any direct linkages to those climate indices related to the variations of LFTY genesis location, such as the PDO, LAT, LON, NPD, TUTT-MT, IPO and Mega-ENSO indices (Figure 3 and Table S2). However, this is not surprising since the LFTY frequency depends largely on the appropriate steering flow (e.g., Li et al., 2017; Tu & Chen, 2019). It is well known that the steering flow can affect the TC tracks, in other words, whether a typhoon could be landed in China depends largely on the steering flow pattern.

For example, typhoons forming in the tropical western North Pacific often tend to be steered by easterly/southeasterly flows (often associated with WNPSH), such prevailing typhoon tracks favor TCs/typhoons to move northwestward to southeastern China (Tu & Chen, 2019). Moreover, in the paper of Li et al. (2017), there was a sentence wrote roughly that: “variations of TC track and landfall position are predominantly governed by the changes in steering flows.” Besides, according to their studies, they

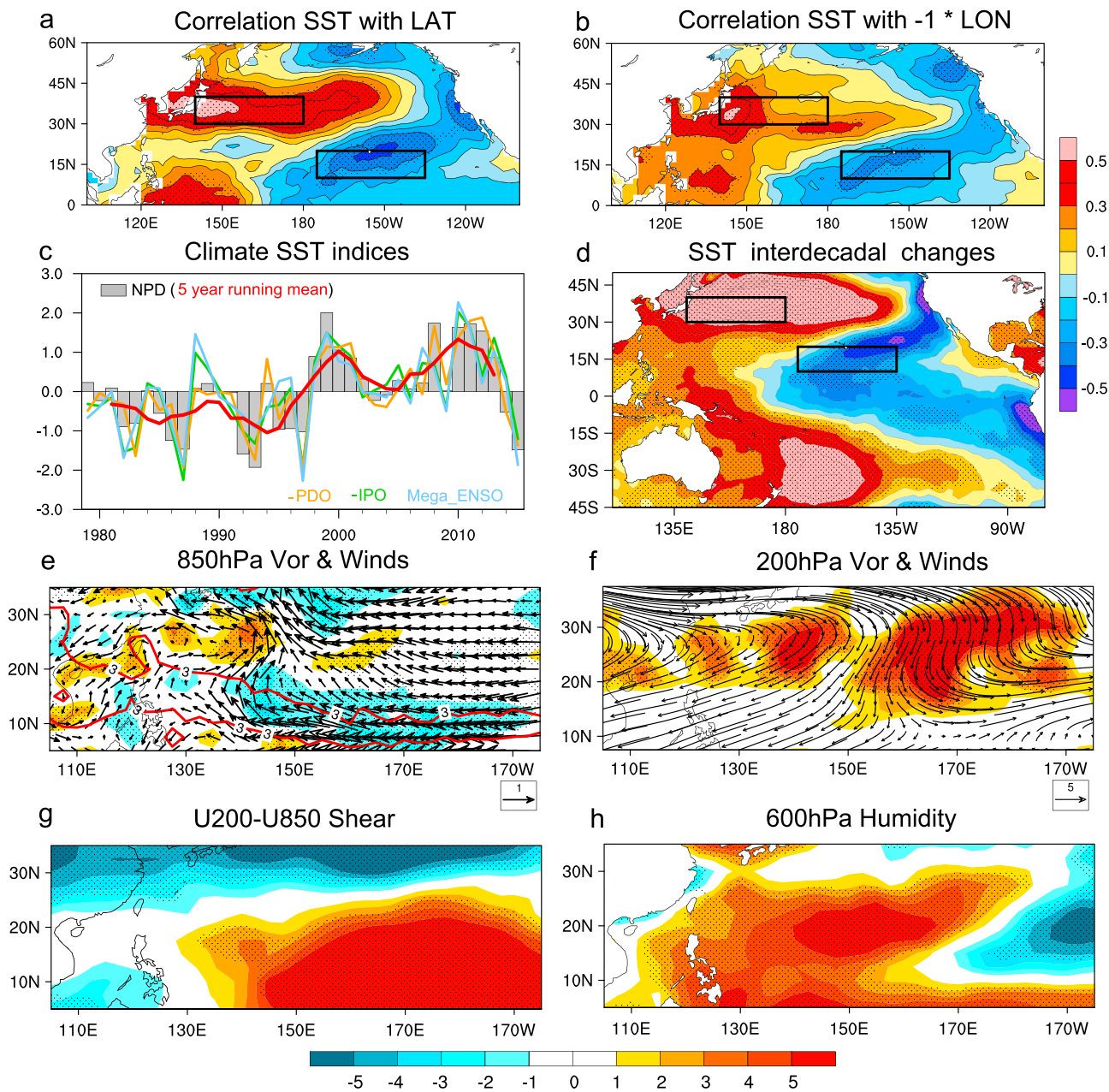


**Figure 2.** Correlations of SST anomalies with the normalized (a) LAT and (b) LON. (c) four normalized SST indices: PDO (orange), IPO (green), Mega-ENSO (blue), NPD [gray bar, defined as the anomaly SST gradient between the two boxes outlined in (a): ( $30^{\circ}$ N- $40^{\circ}$ N,  $140^{\circ}$ E- $180^{\circ}$ E) minus ( $10^{\circ}$ N- $20^{\circ}$ N,  $175^{\circ}$ W- $135^{\circ}$ W)] and its 5-year running mean (red). Interdecadal climate differences of (d) SST ( $^{\circ}$ C), (e) 850 hPa relative vorticity (Vor850, shading,  $10^{-6}/s$ ) & wind (vector, m/s), (f) 200 hPa cyclonic vorticity (Vor200, shading,  $10^{-6}/s$ ), (g) vertical wind shear (U200-U850, m/s) and (h) 600 hPa relative humidity (%) between two equal length periods of 1998-2013 and 1982-1997. The dotted areas indicate the 90% confidence level. The climatological monsoon trough (identified as the Vor850 =  $3 \times 10^{-6}/s$ , red line) and 200 hPa streamlines (m/s, vector) also shown in (e) and (f), respectively. Here the TUTT-MT index is defined as the area-mean of Vor200 anomalies over the ( $170^{\circ}$ E- $175^{\circ}$ W,  $12.5^{\circ}$ N- $17.5^{\circ}$ N) minus the area-mean of Vor850 anomalies over the ( $150^{\circ}$ E- $175^{\circ}$ E,  $10^{\circ}$ N- $15^{\circ}$ N).

concluded that changes in the steering flow pattern tend to affect the subsequent landfall of TCs over southeastern China, resulting in changes in landfall frequency. Hence, it is not surprising that the steering flow could inevitably affect the LFTY frequency over southeastern China.

Accordingly, to unearth the reason for the variations of LFTY frequency, Figure 4 shows the leading EOF modes of the locally steering flow and the relevant circulation anomalies. The EOF1 mode is a dipole

Correlations	PDO	LAT	LON	NPD	TUTT-MT	LFTY	PC2	PC1	EASM	ENSO
PDO	1.00	-0.50	0.30	-0.90	-0.64					0.51
Latitude (LAT)	-0.50	1.00	-0.43	0.53	0.44					
Longitude (LON)	0.30	-0.43	1.00	-0.36	-0.34					
NPD	-0.90	0.53	-0.36	1.00	0.66		-0.31			-0.52
TUTT-MT index	-0.64	0.44	-0.34	0.66	1.00					-0.53
LFTY Frequency						1.00	0.54			
PC2				-0.31		0.54	1.00			
PC1								1.00	0.98	-0.47
EASM								0.98	1.00	-0.42
ENSO (ONI)	0.51			-0.52	-0.53			-0.47	-0.42	1.00
Omit $ r  < 0.275$										
Confidence level										
level 90% 95% 99% 99.9% $ r  > 0.7$ $r = 1.00$										

**Figure 3.** Correlation matrix of 10 indices: PDO, LAT, LON, NPD, TUTT-MT, LFTY frequency (LFTY), PC1 & PC2 (as shown in Figure 4), ENSO and EASM (Wang & Fan, 1999). Only the correlations exceeding the estimated 90% confidence level are shown.

(Figure 4(a)), similar to the definition of East Asian summer monsoon (EASM) proposed by Wang and Fan (1999). As expected, the correlation between PC1 and EASM is robust, high upon 0.98 (Figures 3 and 4(b)). Hence the EOF1 is recognized as the leading mode of EASM, highlighting an intensified WNP anticyclone (Figure 4(e)) that is traditionally linked to ENSO (Figures 3).

In contrast, the EOF2 mode highlight the enhanced easterly airflows near the 20°N over the South China Sea and the Philippine Sea (Figure 4(c)). The corresponded PC2 is significantly correlated to the LFTY frequency ( $R = 0.54$ , exceeding the 99.9% confidence level; Figures 3 and 4(d)); and the associated circulation pattern exhibits an anomalous anticyclone centered over the East China Sea and two weak cyclone over the southwestern WNP (Figure 4(f)). This is an indirect reflection of the strengthened Hadley circulation accompanied with the enhanced tropical convection and WNPSH (Figure S2 and Figure 4(f)). The corresponding easterly steering flows (Figure 4f) shed light on the reason why relatively more typhoons landfalling on southern China during period II (Figure 4(d), Figure 1(e) vs. Figure 1(f)). In other words, it is the necessary condition for the northwestward movement-and-landfall of typhoons that there are continuing easterly steering flows near the 20°N on the southwest side of WNPSH.

#### 4. Discussion

It should be noticed that Zhan and Wang (2017) recently pointed out that the weak TCs (with maximum sustained surface wind speed less than 33 m/s) dominate the poleward shift of the mean location of lifetime maximum intensity of WNP TCs since 1980. This is found to be considerably linked to the significant increasing (decreasing) trend of TC genesis in the northwestern (southern) WNP during recent decades. In other words, the northwestward shifts of WNP TCs are mainly contributed from the increasing weak TCs north of the 20°N (as shown in the Figure 2 of He et al., 2015). Of note is that here the identified LFTYs are all intense TCs and mostly generated over south of 20°N (i.e., southern WNP, Figure 1(b)). Although the interdecadal changes in TC genesis location and frequency as well as in the proportion of intense TC over the WNP have been well attributed to the IPO- and/or Mega-La Niña-related climate shift by many previous studies (e.g., Zhan et al., 2017; J. Zhao, Zhan, Wang, & Xu, 2018; C. Hu, Zhang, et al., 2018 and their references), however, attributions of the frequency and genesis-location changes in LFTY dedicated to southern China remain unclear. Hence, this study focuses on the LFTYs that meet the following two criterions:

1. The intense TCs with maximum sustained surface wind speed  $\geq 64$  knots ( $\approx 33$  m/s);
2. Landfalling typhoons dedicated to southern China.

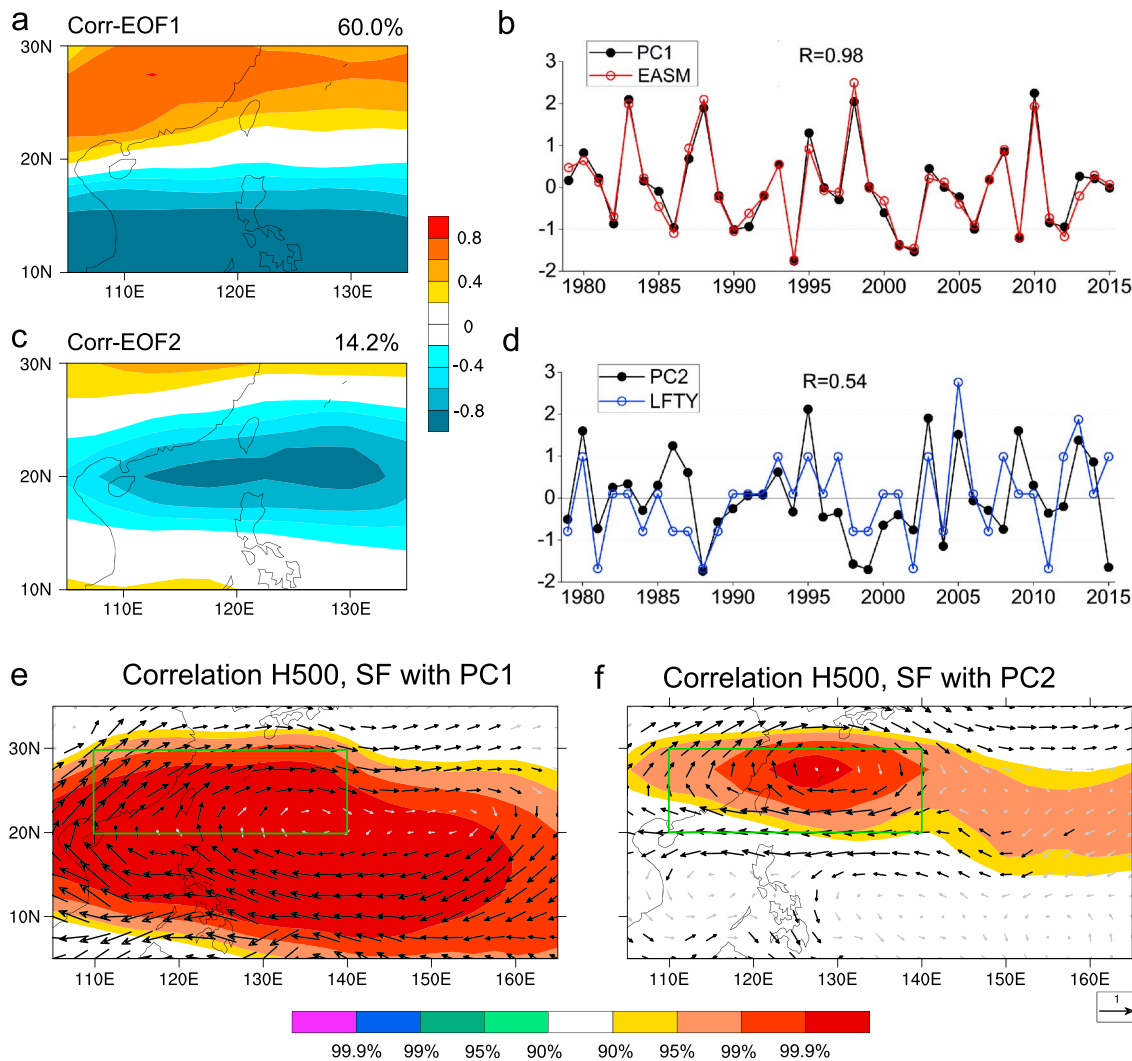


**Figure 4.** (a) EOF1 and (c) EOF2 of zonal steering flow anomalies are shown as the correlation patterns with the normalized (b) PC1 and (d) PC2. Shown in (e) and (f) are the correlation maps of H500 (shading) and steering flow (SF, vector) anomalies (only shading above the 90% confidence level). Besides, normalized EASM index (Wang & Fan, 1999) and LFTY frequency are also shown in (b) and (d), respectively. The green boxes in (e) and (f) are the same as in Figure 1(e) and (f).

Statistic mean results show that only about 31.9% of WNP typhoons could make landfall over southern China during the most active typhoon season (JAS, Figures 1(a)), but LFTY-induced consequences are grossly incalculable. Accordingly, it is necessary to conduct a separate study on the variations of southern China typhoon from the perspective of landfalling frequency and genesis location.

## 5. Concluding Remarks

Our straightforward results reveal that changes in the genesis location and landfalling frequency of southern China typhoon are affected by different climate factors. The main conclusions are as follows:

First, most southern China LFTYs are mainly formed south of 20°N; and their mean latitude and longitude of genesis locations together show a robust interdecadal northwestward shift since the late-1990s (Figure 1(c)-1(d)), both are significantly correlated with the North Pacific SST dipole anomalies (NPD, Figures 2(a)-2(b)) that are mainly induced by the late-1990s Pacific Mega-La Niña-like climate regime shift (Figure 3, Table S2).

Second, the PDO-related Mega-La Niña-like climate shift modulate the mean LFTY genesis location mainly via affecting the *tacit-and-mutual configurations* between TUTT and MT (Figures 2(c)-2(d)), as well as the

resultant vertical wind shear and mid-level relative humidity anomalies (Figures 2(e)-2(f)), consisting with previous studies (e.g., Camargo et al., 2007; C. Hu, Zhang, et al., 2018; Huangfu et al., 2017; H. Zhao, Duan, et al., 2018; Wu et al., 2015).

Third, the LFTY frequency has slightly increased (albeit insignificant) in recent decades (Figures 1(c)-1(d)) without directly linkages to the PDO and ENSO (Figure 3). Variations of LFTY frequency are primarily attributed to the effects of the anomalous easterly steering flows near the 20°N over the South China Sea and the Philippine Sea (Figure 4), which are closely linked to the WNPSH activity. Above results have certain reference value for southern China LFTY prediction from the short-term climate perspective. Finally, it could be projected that such Mega-La Niña-like interdecadal climate changes, if continuing, would inevitably increase the risks of intense LFTY over the WNP (e.g., Mei & Xie, 2016; Zhan et al., 2017; H. Zhao, Duan, et al., 2018). Fortunately, maybe the positive phase PDO (corresponding to Mega-El Niño) is worthwhile looking forward to the ongoing decade (<http://research.jisao.washington.edu/pdo/PDO.latest.txt>), which has begun since 2014.

## Acknowledgments

The atmospheric datasets of ERA-Interim are obtained from the ECMWF (<http://apps.ecmwf.int/datasets/>); and the ERSST-v4 & HadISST data sets are available at the following two URLs, respectively: <https://www.esrl.noaa.gov/psd/> and <https://www.metoffice.gov.uk/hadobs/hadisst/>. This research is supported by the National Natural Science Foundation of China (41465003, 41705050, 41690121, 41690123, 41690120, 41875101, 41805054 and 41665006), and the National Postdoctoral Program for Innovative Talents (BX201600039).

## References

- Camargo, S. J., Emanuel, K. A., & Sobel, A. H. (2007). Use of a genesis potential index to diagnose ENSO effects on tropical cyclone genesis. *Journal of Climate*, 20(19), 4819–4834. <https://doi.org/10.1175/JCLI4282.1>
- Chan, J. C. L. (2008). Decadal variations of intense typhoon occurrence in the western North Pacific. *Proceedings of the Royal Society A: Mathematical, Physical and Engineering Sciences*, 464(2089), 249–272. <https://doi.org/10.1098/rspa.2007.0183>
- Chan, K. T. F., Chan, J. C. L., & Wong, W. K. (2019). Rainfall asymmetries of landfalling tropical cyclones along the South China coast. *Meteorological Applications*, 26(2), 213–220. <https://doi.org/10.1002/met.1754>
- Dee, D. P., Uppala, S. M., Simmons, A. J., Berrisford, P., Poli, P., Kobayashi, S., et al. (2011). The ERA-interim reanalysis: Configuration and performance of the data assimilation system. *Quarterly Journal of the Royal Meteorological Society*, 137(656), 553–597. <https://doi.org/10.1002/qj.828>
- Emanuel, K. A., & Nolan, D. (2004). Tropical cyclone activity and global climate. In *26th Conference on Hurricanes and Tropical Meteorology* (pp. 240–241). Miami, FL: American Meteorological Society.
- Guo, Y.-P., & Tan, Z.-M. (2018). Westward migration of tropical cyclone rapid-intensification over the northwestern Pacific during short duration El Niño. *Nature Communications*, 9(1), 1507. <https://doi.org/10.1038/s41467-018-03945-y>
- He, H., Yang, J., Gong, D., Mao, R., Wang, Y., & Gao, M. (2015). Decadal changes in tropical cyclone activity over the western North Pacific in the late 1990s. *Climate Dynamics*, 45(11–12), 3317–3329. <https://doi.org/10.1007/s00382-015-2541-1>
- Henley, B. J., Gergis, J., Karoly, D. J., Power, S., Kennedy, J., & Folland, C. K. (2015). A tripole index for the Interdecadal Pacific oscillation. *Climate Dynamics*, 45(11–12), 3077–3090. <https://doi.org/10.1007/s00382-015-2525-1>
- Hong, C.-C., Li, Y.-H., Li, T., & Lee, M.-Y. (2011). Impacts of Central Pacific and eastern Pacific El Niños on tropical cyclone tracks over the western North Pacific. *Geophysical Research Letters*, 38, L16712. <https://doi.org/10.1029/2011GL048821>
- Hong, C.-C., Wu, Y.-K., & Li, T. (2016). Influence of climate regime shift on the interdecadal change of tropical cyclone activity over Pacific Basin during middle to late 1990s. *Climate Dynamics*, 47(7–8), 2587–2600. <https://doi.org/10.1007/s00382-016-2986-x>
- Hu, C., Yang, S., Wu, Q., Zhang, T., Zhang, C., Li, Y., et al. (2016). Reinspecting two types of El Niño: A new pair of Niño indices for improving real-time ENSO monitoring. *Climate Dynamics*, 47(12), 4031–4049. <https://doi.org/10.1007/s00382-016-3059-x>
- Hu, C., Zhang, C., Yang, S., & Chen, D. (2019). Variable correspondence between western North Pacific tropical cyclone frequency and east Asian subtropical jet stream during boreal summer: A tropical Pacific SST perspective. *International Journal of Climatology*, 39(3), 1768–1776. <https://doi.org/10.1002/joc.5905>
- Hu, C., Zhang, C., Yang, S., Chen, D., & He, S. (2018). Perspective on the northwestward shift of autumn tropical cyclogenesis locations over the western North Pacific from shifting ENSO. *Climate Dynamics*, 51(7–8), 2455–2465. <https://doi.org/10.1007/s00382-017-4022-1>
- Hu, F., Li, T., Liu, J., Bi, M., & Peng, M. (2018). Decrease of tropical cyclone genesis frequency in the western North Pacific since 1960s. *Dynamics of Atmospheres and Oceans*, 81, 42–50. <https://doi.org/10.1016/j.dynatmoc.2017.11.003>
- Huang, B., Banzon, V. F., Freeman, E., Lawrimore, J., Liu, W., Peterson, T. C., et al. (2015). Extended reconstructed sea surface temperature version 4 (ERSST.v4). Part I: Upgrades and intercomparisons. *Journal of Climate*, 28(3), 911–930. <https://doi.org/10.1175/JCLI-D-14-0006.1>
- Huangfu, J., Huang, R., Chen, W., Feng, T., & Wu, L. (2017). Interdecadal variation of tropical cyclone genesis and its relationship to the monsoon trough over the western North Pacific. *International Journal of Climatology*, 37(9), 3587–3596. <https://doi.org/10.1002/joc.4939>
- Knutson, T. R., McBride, J. L., Chan, J., Emanuel, K., Holland, G., Landsea, C., et al. (2010). Tropical cyclones and climate change. *Nature Geoscience*, 3(3), 157–163. <https://doi.org/10.1038/ngeo779>
- Li, R. C. Y., Zhou, W., Shun, C. M., & Lee, T. C. (2017). Change in destructiveness of Landfalling tropical cyclones over China in recent decades. *Journal of Climate*, 30(9), 3367–3379. <https://doi.org/10.1175/JCLI-D-16-0258.1>
- Lin, I.-I., & Chan, J. C. L. (2015). Recent decrease in typhoon destructive potential and global warming implications. *Nature Communications*, 6(1), 7182. <https://doi.org/10.1038/ncomms8182>
- Maue, R. N. (2011). Recent historically low global tropical cyclone activity. *Geophysical Research Letters*, 38, L14803. <https://doi.org/10.1029/2011GL047711>
- Mei, W., & Xie, S. (2016). Intensification of landfalling typhoons over the Northwest Pacific since the late 1970s. *Nature Geoscience*, 9(10), 753–757. <https://doi.org/10.1038/ngeo2792>
- Mei, W., Xie, S.-P., Primeau, F., McWilliams, J. C., & Pasquero, C. (2015). Northwestern Pacific typhoon intensity controlled by changes in ocean temperatures. *Science Advances*, 1(4), e1500014. <https://doi.org/10.1126/sciadv.1500014>
- Murakami, H., & Wang, B. (2010). Future change of North Atlantic tropical cyclone tracks: Projection by a 20-km-mesh global atmospheric model. *Journal of Climate*, 23(10), 2699–2721. <https://doi.org/10.1175/2010JCLI3338.1>

- Peduzzi, P., Chatenoux, B., Dao, H., de Bono, A., Herold, C., Kossin, J., et al. (2012). Global trends in tropical cyclone risk. *Nature Climate Change*, 2(4), 289–294. <https://doi.org/10.1038/nclimate1410>
- Rayner, N. A., Parker, D. E., Horton, E. B., Folland, C. K., Alexander, L. V., Rowell, D. P., et al. (2003). Global analyses of sea surface temperature, sea ice, and night marine air temperature since the late nineteenth century. *Journal of Geophysical Research*, 108(D14), 4407. <https://doi.org/10.1029/2002JD002670>
- Seo, N. S., & Bakkensen, L. A. (2017). Is tropical cyclone surge, not intensity, what kills so many people in South Asia? *Weather, Climate, and Society*, 9, 71–81.
- Takahashi, C., Watanabe, M., & Mori, M. (2017). Significant aerosol influence on the recent decadal decrease in tropical cyclone activity over the western North Pacific. *Geophysical Research Letters*, 44, 9496–9504. <https://doi.org/10.1002/2017GL075369>
- Tu, J., & Chen, J. (2019). Large-scale indices for assessing typhoon activity around Taiwan. *International Journal of Climatology*, 39(2), 921–933. <https://doi.org/10.1002/joc.5852>
- Wang, B., & Fan, Z. (1999). Choices of south Asian summer monsoon indices. *Bulletin of the American Meteorological Society*, 80(4), 629–638. [https://doi.org/10.1175/1520-0477\(1999\)080<0629:COSASM>2.0.CO;2](https://doi.org/10.1175/1520-0477(1999)080<0629:COSASM>2.0.CO;2)
- Wang, B., Liu, J., Kim, H. J., Webster, P. J., Yim, S. Y., & Xiang, B. (2013). Northern hemisphere summer monsoon intensified by mega-El Niño/southern oscillation and Atlantic multidecadal oscillation. *Proceedings of the National Academy of Sciences of the United States of America*, 110(14), 5347–5352. <https://doi.org/10.1073/pnas.1219405110>
- Wang, C., & Wu, L. (2016). Interannual shift of the tropical upper-tropospheric trough and its influence on tropical cyclone formation over the Western North Pacific. *Journal of Climate*, 29(11), 4203–4211. <https://doi.org/10.1175/JCLI-D-15-0653.1>
- Wang, C., & Wu, L. (2018). Projection of North Pacific tropical upper-tropospheric trough in CMIP5 models: Implications for changes in tropical cyclone formation locations. *Journal of Climate*, 31(2), 761–774. <https://doi.org/10.1175/JCLI-D-17-0292.1>
- Weinkle, J., Maué, R., & Pielke, R. J. (2012). Historical global tropical cyclone landfalls. *Journal of Climate*, 25(13), 4729–4735. <https://doi.org/10.1175/JCLI-D-11-00719.1>
- Woodruff, J. D., Irish, J. L., & Camargo, S. J. (2013). Coastal flooding by tropical cyclones and sea-level rise. *Nature*, 504(7478), 44–52. <https://doi.org/10.1038/nature12855>
- Wu, L., & Wang, C. (2015). Has the Western Pacific subtropical high extended westward since the late 1970s? *Journal of Climate*, 28(13), 5406–5413. <https://doi.org/10.1175/JCLI-D-14-00618.1>
- Wu, L., Wang, C., & Wang, B. (2015). Westward shift of western North Pacific tropical cyclogenesis. *Geophysical Research Letters*, 42, 1537–1542. <https://doi.org/10.1002/2015GL063450>
- Wu, L., & Zhao, H. (2012). Dynamically derived tropical cyclone intensity changes over the western North Pacific. *Journal of Climate*, 25(1), 89–98. <https://doi.org/10.1175/2011JCLI4139.1>
- Wu, X. (2019). What are the impacts of tropical cyclones on employment? An analysis based on meta-regression. *Weather, Climate, and Society*, 11(2), 259–275. <https://doi.org/10.1175/WCAS-D-18-0052.1>
- Zhan, R., & Wang, Y. (2017). Weak tropical cyclones dominate the poleward migration of the annual mean location of lifetime maximum intensity of Northwest Pacific tropical cyclones since 1980. *Journal of Climate*, 30(17), 6873–6882. <https://doi.org/10.1175/JCLI-D-17-0019.1>
- Zhan, R., Wang, Y., & Zhao, J. (2017). Intensified Mega-ENSO has increased the proportion of intense tropical cyclones over the western Northwest Pacific since the late 1970s. *Geophysical Research Letters*, 44, 11,959–11,966. <https://doi.org/10.1002/2017GL075916>
- Zhao, H., Duan, X., Raga, G. B., & Klotzbach, P. J. (2018). Changes in characteristics of rapidly intensifying western North Pacific tropical cyclones related to climate regime shifts. *Journal of Climate*, 31(19), 8163–8179. <https://doi.org/10.1175/JCLI-D-18-0029.1>
- Zhao, H., Jiang, X., & Wu, L. (2015). Modulation of Northwest Pacific tropical cyclone genesis by the intraseasonal variability. *Journal of the Meteorological Society of Japan*, 93(1), 81–97. <https://doi.org/10.2151/jmsj.2015-006>
- Zhao, H., & Wu, L. (2014). Inter-decadal shift of the prevailing tropical cyclone tracks over the western North Pacific and its mechanism study. *Meteorology and Atmospheric Physics*, 31(19), 8163–8179. <https://doi.org/10.1175/JCLI-D-14-0029.1>
- Zhao, H., & Wu, L. (2018). Modulation of convectively coupled equatorial Rossby wave on the western North Pacific tropical cyclones activity. *International Journal of Climatology*, 38(2), 932–948. <https://doi.org/10.1002/joc.5220>
- Zhao, H., Yoshida, R., & Raga, G. B. (2015). Impact of the Madden-Julian Oscillation on western North Pacific tropical cyclogenesis associated with large-scale patterns. *Journal of Applied Meteorology and Climatology*, 54(7), 1413–1429. <https://doi.org/10.1175/JAMC-D-14-0254.1>
- Zhao, J., Zhan, R., & Wang, Y. (2018). Global warming hiatus contributed to the increased occurrence of intense tropical cyclones in the coastal regions along East Asia. *Scientific Reports*, 8(1), 6023. <https://doi.org/10.1038/s41598-018-24402-2>
- Zhao, J., Zhan, R., Wang, Y., & Xu, H. (2018). Contribution of Interdecadal Pacific oscillation to the recent abrupt decrease in tropical cyclone genesis frequency over the western North Pacific since 1998. *Journal of Climate*, 31(20), 8211–8224. <https://doi.org/10.1175/JCLI-D-18-0202.1>